scientific reports

Check for updates

OPEN

# Influence of heat generation/absorption and stagnation point on polystyrene–$TiO_2/H_2O$ hybrid nanofluid flow

Sadaf Masood[1]✉, Muhammad Farooq[2] & Aisha Anjum[3]

**This article focuses on hybrid nanofluid flow induced by stretched surface. The present context covers stagnation point flow of a hybrid nanofluid with the effect of heat generation/absorption. Currently most famous class of nanofluids is Hybrid nanofluid. It contains polystyrene and titanium oxide as a nanoparticles and water as a base fluid. First time attributes of heat transfer are evaluated by utilizing polystyrene–$TiO_2/H_2O$ hybrid nanofluid with heat generation/absorption. Partial differential equations are converted into ordinary differential equation by using appropriate transformations for heat and velocity. Homotopy analysis method is operated for solution of ordinary differential equations. Flow and heat are disclosed graphically for unlike parameters. Resistive force and heat transfer rate is deliberated mathematically and graphically. It is deduced that velocity field enhanced for velocity ratio parameter whereas temperature field grows for heat generation/absorption coefficient. To judge the production of any engineering system entropy generation is also calculated. It is noticed that entropy generation grows for Prandtl number and Eckert number while it shows opposite behavior for temperature difference parameter.**

Heat transmission plays a vital role in many respects for instance in refrigeration, power generation, thermoelectric devices, heat exchangers, roofing materials, food processing, radiative cooling and thermal energy storage etc. Therefore it is advantageous to enhance the production of heat transfer machines adopted in these areas. Thermal conductivity is the crucial framework in heat transfer problems. Ethylene glycol, water and oils have low thermal conductivity. Nanomaterials like oxides of metals, carbides etc. are included in the host fluid for intensification of thermal conductivity. Choi[1] instigated about nanofluids. Hybrid nanofluids seeks the intention of researchers and scientists currently. It consists of two or more non-identical particles having size less than 100 nm. Here, we take polystyrene and titanium oxide as nanoparticles due to their wide use in pharmaceuticals, automotive industry, IT equipments (TV, Computers, laptops), food packing industry, construction, household industry, cosmetics, fabrics and textiles. Waini et al.[2] avails bvp4c to conclude the heat transfer of hybrid nanofluid with shear flow. They checked the stability of a solutions and concluded that one solution is stable from the dual solutions. Influence of CNT—$Fe_3O_4/H_2O$ hybrid nanofluid on infinite rotating disk was studied by Tassaddiq et al.[3]. They observed that heat transfer of CNT—$Fe_3O_4/H_2O$ hybrid nanofluid is greater as compared with $Fe_3O_4/H_2O$. Tayebi et al.[4] analyzed the attributes of hybrid nanofluid (containing Cu and $Al_2O_3$ nanoparticles) bounded by elliptical cylinders with natural convection. He investigated that entropy generation grows for higher Rayleigh number. Peristaltic flow of hybrid nanofluid with entropy generation was executed by Zahid et al.[5]. Shooting method is utilized to perceive numerical solutions. It is noticed that enhanced Hall parameter decays the heat transfer rate as well as entropy generation. Yusuf et al.[6] takes stretching sheet with nonlinear radiations on hybrid nanofluid and investigated that entropy generation rate rises for radiation parameter. Wanatasanapan et al.[7] takes temperature range 30–70 °C and fixed volume fraction 1.0% of $TiO_2$ and $Al_2O_3$ particles. They concluded that hybrid nanofluid with 50:50 ratio at 70 °C has maximum thermal conductivity. Matlab was used by Said et al.[8] for hybrid nanofluid at distinct concentrations. Enhanced nanoparticle volume concentration grows the entropy generation. 19.14% thermal conductivity enhancement was noticed at 60 °C. Abbas et al.[9] considered a hybrid nanofluid in a moving cylinder with slip and inclined MHD. Consequences of silver-$CuO/H_2O$ nanofluid with stagnation point and stretching sheet are discussed by Arani et al.[10]. They used R–K method with shooting technique. They conclude

[1]Department of Mathematics, Riphah International University, Islamabad 44000, Pakistan. [2]Department of Mathematics and Statistics, University of Haripur, Haripur, Pakistan. [3]Department of Mathematics, NUML, Islamabad, Islamabad, Pakistan. ✉email: maliksadafirfan12@gmail.com

that heat transfer rate grows 100% for hybrid nanofluid with suction/injection parameter. Enhancement of heat transfer in a car radiator with hybrid nanofluid was studied by Li et al.[11]. He found that at 0.4% volume fraction 32.01% thermal conductivity rises. Waini et al.[12,13] disclosed the impact of surface heat flux and stagnation point on a stretching/shrinking cylinder filled with a hybrid nanofluid. They also studied about squeezed flow over a permeable sensor surface. Results showed that unique solution was obtained for $\lambda \geq -1$. They also conclude that the first solution is stable only. Different researchers take polystyrene and titanium oxide nano particles and perform numerous experiments[14–18].

Excessive applications of stagnation point flow of Newtonian as well as Non-Newtonian fluid seeks the researchers intention. A point where fluid is static by the object is called stagnation point. It is classified as oblique and orthogonal stagnation point. Stagnation point undergoes a highest pressure and highest heat transmission. Innumerable applications of stagnation point flows in engineering, home industry, aerodynamic industry and in metallurgy are noticed. They include cooling of plates, nuclear reactor cooling, tinning of wires and wire drawing etc. Naganthran et al.[19] described the flow of viscoelastic fluid past a shrinking sheet with oblique stagnation point. They concluded that enhanced mass flux parameter strengthens the heat transfer rate. Consequences of chemical reaction on CNTs along with stagnation point was founded by Khan et al.[20]. Magnified velocity ratio parameter decays the drag force. Ascendancy of Maxwell fluid with suction/injection was illustrated by Ahmed et al.[21]. Porous rotating disk was also considered. Numerical results showed that rotation parameter enhanced the Nusselt number at the surface. Moshkin et al.[22] elaborated the flow of unsteady Maxwell fluid by transforming the equations into the Lagrangian coordibates. Weidman[23] contemplated a flow along a rotating plate and revealed the influence of Hiemenz stagnation point on this plate. He gave good comparision with Hannah's consideration. The out turn of Homann stagnation point on a non-Newtonian fluid regarding a stable plate was initiated by Mahapatra et al.[24]. They deduced that viscoelastic parameter grows the velocity profile. Azhar et al.[25] studied about heat generation and viscous dissipation of Jeffrey fluid along with stagnation point. Stretching ratio parameter enhanced the drag force as well as Sherwood number. Flow of MHD Carreau fluid induced by stretching surface was instigated by Chu et al.[26]. He examined flow about stagnation point. Both heat and mass will transfer more fastly by increasing velocity ratio parameter. Shah et al.[27] takes a Riga plate and found the out turns of stagnation point and mixed convection along with porous medium. Darcy number decays the velocity field while grows the skin friction. Awan et al.[28] assumed MHD second grade fluid with oblique stagnation point. The flow was induced by oscillatory surface. He showed that Sherwood number and heat transfer rate boosts up for larger suction parameter. Effect of stagnation point on Cu–$Al_2O_3$/water hybrid nanofluid with shrinking cylinder was investigated by Waini et al.[29]. The findings revealed that velocity grows for rising Reynold number. Influence of mixed convection flow on hybrid nanofluid flow with stagnation point was originated by Zainal et al.[30]. They concluded that heat transfer rate and skin friction coefficient boosts up for growing suction parameter.

The fluid flows initiated by stretching surfaces have significant preferences in engineering as well as industrial applications. For example, cooling of stripes, glass fiber, extrusion processes, paper production, drawing of paper film, crystal growth and production of rubber sheets etc. To obtain output of acceptable quality stretching and cooling of sheets played an important role. In past, many researchers investigated the flow induced by stretching sheets. Buoyancy effects on hybrid nanofluid flow over an exponentially stretching sheet with stagnation point was scrutinized by Waini et al.[31]. They considered $Al_2O_3$–Cu/Water hybrid nanofluid and bvp4c Matlab solver for finding the solution of the problem. They noticed that first solution of heat transfer coefficient increased for greater mixed convection parameter. Khashi'ie et al.[32] examined the dual solutions of hybrid nanofluid with prescribed heat flux. They assumed cylinder as well as flat plate and found the results. Bvp4c Matlab solver was employed. They obtained that concentration of Alumina particles $\Phi_1 = 0.5\%$ and concentration of copper particles $\Phi_2 = 1.5\%$ has extortionate heat transfer rate. Similarly Zainal et al.[33–35] considered hybrid nanofluid with viscous dissipation, stagnation point and velocity slip effects. They also take exponentially stretching sheet with quadratic velocity and gained different remarkable results.

The crucial element in industrial, geographical and engineering processes is transmission of heat. They include numerous applications such as thermal insulation, geothermal supplies, cooling of electrical devices, metal casting etc. The temperature difference within a body is the key factor for heat generation/absorption. Two dimensional flow of Oldroyd-B fluid with heat generation/absorption under Cattaneo–Christov approach was developed by Ibrahim et al.[36]. They utilized finite element method for solution of the problem. The results revealed that heat transfer rate enhanced for increased heat generation/absorption parameter. Outcomes of hybrid nanofluid over exponentially stretching sheet with heat generation was examined by Zainal et al.[37]. Suction parameter strengthens the rate of heat transfer. Hafeez et al.[38] considered a rotating disk having Oldroyd-B fluid with the influence of heat generation/absorption. They concluded that the temperature is an increasing function for magnetic number whereas it decays for thermal relaxation time parameter. Consequences of heat generation/absorption on hybrid nanofluid in a circular annulus was founded by Tayabi et al.[39]. They take Cu and $Al_2O_3$ as nanoparticles. They found that the influence of IHG/A modifies the heat exchange rate in the annulus.

Conception of entropy in thermodynamic system was prescribed by Rudolf Clausius in 1850s. It is the amount of thermal energy per unit temperature which is unattainable for performing beneficial tasks. The quantity of entropy assembled in irreversible processes is termed as entropy production. For example heat exchange, heat engines, fluid flows, heat pumps, power plants, air conditioners and refrigeration etc. It determines the execution of thermodynamical system. At first Bejan[40] studied about entropy generation. He explained the significant steps of entropy depreciation. Gholamalipour et al.[41] studied the entropy generation of nanofluid in a permeable annulus. For lesser Darcy and Rayleigh number greater disturbance in entropy production is noticeable. Dutta et al.[42] considered a rhombic shape closed pattern pervaded by Cu–water nanofluid and investigates about entropy generation. He showed that increment in Ha decays the entropy production rate. Khan et al.[43] discussed the impact of joule heating on Casson fluid passing through a revolving cylinder. Entropy generation shows increasing trend for larger Brinkman number. Attributes of entropy production in Newtonian fluid with Darcy

model was analyzed by Ambreen et al.[44]. Cho[45] takes a square cavity whose some walls are heated and filled it by Cu–water nanofluid. Along this he considered a porous medium inside the cavity and then measure the entropy production rate. For a fixed Rayleigh number, entropy rate enhanced with enlarged Darcy number. Influence of natural convection in elliptical cavity pervaded by hybrid nanofluid was inspected by Tayebi et al.[4]. Zahid et al.[5] explained that low entropy production occurs for higher Hall parameter. Li et al.[46] examined the thermal radiation effect in a tilted square cavity. He also analyzed the entropy production rate here and found that Rayleigh number grows the entropy production rate. Sachica et al.[47] scrutinized the $Al_2O_3$–water nanofluid in a rectangular channel and numerically investigate it. Nano particle volume fraction decreases the entropy generation rate.

Extraordinary enhancement in thermal conductivity is noticed for hybrid nanofluids in comparision with ordinary nanofluids. Therefore have innumerable applications in home industry, automotive industry, engineering, for cancer treatment, cosmetics, pharmaceuticals, food pakaging, paper plastics, fabrics, ceramics, paints, food colorants and in soaps as well. Here the key objective is to discuss the characteristics of polystyrene–$TiO_2$/$H_2O$ hybrid nanofluid flow with heat generation/absorption. Stagnation point is also contemplated in momentum equation. We take advantage of congrous transformations for transmutation of partial differential equations into non dimensionalized ordinary differential equations. Homotopic methodology[48–54] is executed for series solution. Ramification of incompatible parameters are interpreted graphically. Mathematical expression of drag force is calculated and Nusselt number is manifested graphically. Entropy generation rate is also exposed through graphs.

## Formulation

Analysis of two dimensional hybrid nanofluid suppressed with polystyrene and titanium oxide ($TiO_2$) particles has carried out. Influence of stagnation point on flow pattern is also discussed. Impact of heat generation/absorption is also figure out. We take stretching velocity $u = U_w(x) = ax$ at $y = 0$. Free stream velocity $u = U_e(x) = bx$ is considered at $y \to \infty$. Persistent temperature is presumed at both plate surface and ambient fluid.

After implementation of boundary layer approximation the ruling equations appears as[55]:

$$\frac{\partial u}{\partial x} + \frac{\partial v}{\partial y} = 0, \tag{1}$$

$$u\frac{\partial u}{\partial x} + v\frac{\partial u}{\partial y} = U_e\frac{dU_e}{dx} + \upsilon_{hnf}\frac{\partial^2 u}{\partial y^2}, \tag{2}$$

$$u\frac{\partial T}{\partial x} + v\frac{\partial T}{\partial y} = \alpha_{hnf}\frac{\partial^2 T}{\partial y^2} + (T - T_\infty)\frac{Q}{\left(\rho C_p\right)_{hnf}}, \tag{3}$$

here $u$ and $v$ are symbolized as velocity constituents $x$ and $y$ respectively. $U_e$ designated as free stream velocity, $\upsilon_{hnf}$ stands for kinematic viscosity of hybrid nanofluid, $\rho_{hnf}$ characterizes density of hybrid nanofluid, heat capacity of hybrid nanofluid is denoted by $\left(\rho C_p\right)_{hnf}$, $\alpha_{hnf}$ indicates thermal diffusivity of hybrid nanofluid. $T$ stands for fluid temperature.

Corresponding boundary conditions are

$$u = U_w(x) = ax, v = 0, T = T_0 + dx^2, \text{ at } y = 0, \tag{4}$$

$$u = U_e(x) = bx, T \to T_\infty, \text{ at } y \to \infty. \tag{5}$$

here $u$ and $v$ denotes velocity components, $U_w(x)(= ax)$ stands for stretching velocity, $T_0$ denotes reference temperature, $T_w$ is the temperature of plate, ambient temperature is represented by $T_\infty$.

Exploiting the transformations[56]

$$u = axf'(\eta), v = -\sqrt{a\nu}f(\eta), \eta = \sqrt{\frac{a}{\nu}}y, \theta(\eta) = \frac{T - T_\infty}{T_w - T_\infty}, \tag{6}$$

Equation (1) is fulfilled consistently. Though Eqs. (2–5) appears as:

$$f''' - B(1 - \Phi_1)^{2.5}(1 - \Phi_2)^{2.5}((f')^2 - ff'') + A^2 = 0, \tag{7}$$

$$\left(\frac{B_1}{\Pr}\theta'' + \lambda\theta\right)\frac{1}{D_1} + f\theta' - 2\theta f' = 0, \tag{8}$$

$$f'(0) = 1,\ f(0) = 0,\ f'(\infty) = A, \tag{9}$$

$$\theta(0) = 1,\ \theta(\infty) = 0, \tag{10}$$

In these equations $A$ denotes velocity ratio parameter, Pr symbolizes the Prandtl number, $\lambda$ is heat generation/absorption parameter. Algorithmic representation of these quantities are specified as:

$$A = \frac{b}{a},\ \mathrm{Pr} = \frac{\upsilon}{\alpha},\ \lambda = \frac{Q}{(\rho C_p)_f a}, B_1 = \frac{k_{hnf}}{k_f}, Ec = \frac{u_w^2}{C_p(T_w - T_\infty)},$$
$$B = \left[(1-\Phi_2)\left\{(1-\Phi_1) + \Phi_1\frac{\rho_{s1}}{\rho_f}\right\} + \Phi_2\frac{\rho_{s2}}{\rho_f}\right], \tag{11}$$
$$D_1 = \left[(1-\Phi_2)\left\{(1-\Phi_1) + \Phi_1\frac{(\rho C)_{s1}}{(\rho C)_f}\right\} + \Phi_2\frac{(\rho C)_{s2}}{(\rho C)_f}\right],$$

Mathematical form of drag force is prescribed as:

$$C_f = \frac{\tau_w}{\rho U_w^2}, \tag{12}$$

Non dimensionalized configuration is expressed as

$$C_f Re_x^{1/2} = -\frac{1}{(1-\Phi_1)^{2.5}(1-\Phi_2)^{2.5}} f''(0), \tag{13}$$

Nusselt number is declared as

$$Nu = \frac{x q_w}{k_f(T_w - T_\infty)}, \tag{14}$$

Its undimensional form is as below

$$NuRe_x^{1/2} = -\frac{k_{hnf}}{k_f}\theta'(0), \tag{15}$$

here local Reynolds number is symbolized by $Re_x = U_w(x)x/\nu$.

## Entropy generation

Here our principal focus is to evaluate the irreversibilities of a system through entropy generation. Mathematically it is given as

$$E_G = \frac{k_{hnf}}{(T_\infty)^2}\left(\frac{\partial T}{\partial y}\right)^2 + \frac{\mu_{hnf}}{T_\infty}\left(\frac{\partial u}{\partial y}\right)^2, \tag{16}$$

Dimensionless numerical formula for entropy generation is demonstrated as

$$N_s = \frac{(T_\infty)^2\left(\frac{\eta}{y}\right)^2}{k_{hnf}(T_w - T_\infty)^2} E_G, \tag{17}$$

Achieved non dimensional form is

$$N_s = \theta'^2 + \frac{Ec\ \mathrm{Pr}}{\Omega(1-\Phi_1)^{2.5}(1-\Phi_2)^{2.5}}\frac{k_f}{k_{hnf}} f''^2, \tag{18}$$

Bejan number is expressed as

$$Be = \frac{\text{Entropy generation due to thermal irreversibility}}{\text{Total entropy generation}}, \tag{19}$$

$$Be = \frac{\theta'^2}{\theta'^2 + \frac{Ec\,\mathrm{Pr}}{\Omega(1-\Phi_1)^{2.5}(1-\Phi_2)^{2.5}}\frac{k_f}{k_{hnf}} f''^2}, \tag{20}$$

## Solution methodology

**Homotopic solutions.** Homotopic method was exposed by Liao[48]. This method is utilized for finding the series solutions of highly non-linear problems. It is independent of any small or large parameter. Convergence can be find and control easily. Initial guesses and linear approximations are free to choose. They are intimated as follows:

$$f_0(\eta) = A\eta - (A-1)\big(1 - \exp(-\eta)\big), \tag{21}$$

$$\theta_0(\eta) = exp(-\eta). \tag{22}$$

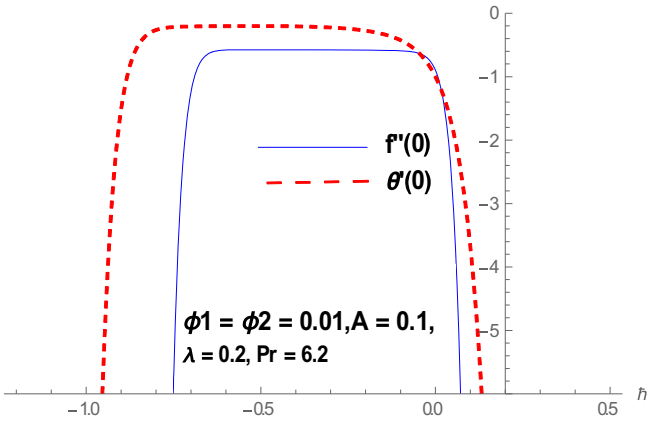


**Figure 1.** h-Curve for $f(\eta)$ and $\theta(\eta)$.

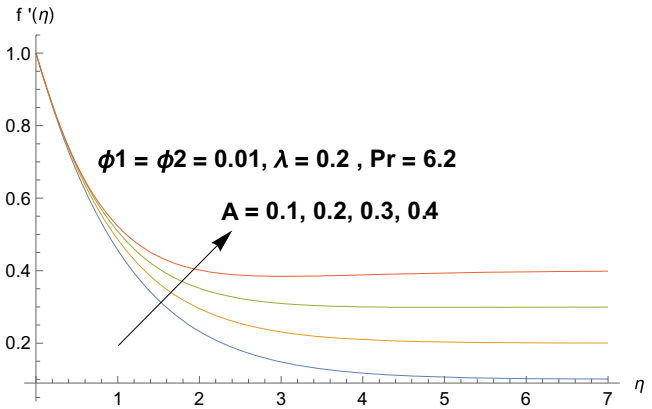


**Figure 2.** Illustration of A on $f'(\eta)$.

$$\mathbf{L}_f(f) = \frac{d^3f}{d\eta^3} + \frac{d^2f}{d\eta^2},\ \mathbf{L}_\theta(\theta) = \frac{d^2\theta}{d\eta^2} - \theta, \tag{23}$$

with

$$\mathbf{L}_f\left[(C_1 + C_2\eta) + C_3\exp(-\eta)\right] = 0, \tag{24}$$

$$\mathbf{L}_\theta\left[C_4\exp(\eta) + C_5\exp(-\eta)\right] = 0, \tag{25}$$

here $C_i(i = 1, \ldots, 5)$ characterizes the arbitrary constants.

The final solutions $(f_m,\ \theta_m)$ with the association of special solutions $(f_m^*(\eta),\ \theta_m^*(\eta))$ are disclosed by

$$f_m(\eta) = f_m^?(\eta) + C_1 + C_2\eta + C_3e^{-\eta}, \tag{26}$$

$$\theta_m(\eta) = \theta_m^?(\eta) + C_4e^{\eta} + C_5e^{-\eta}, \tag{27}$$

**Convergence analysis.** Homotopy analysis method is that method which gave us freedom to choose and control the convergence region. Figure 1 reflects the $\hbar$-curves for $f'(\eta)$ and $\theta(\eta)$. The ranges for $\hbar_f$ and $\hbar_\theta$ are $-0.6 \le \hbar_f \le -0.1$ and $-0.8 \le \hbar_\theta \le -0.5$.

## Discussion

Graphical demonstration of influential parameters for flow and heat transmission are given in this portion. Thus figures are portrayed. Effect of velocity ratio parameter $A$ on velocity profile is illustrated in Fig. 2. It is noticed that both velocity profile and momentum boundary layer thickness enhanced for increased velocity ratio parameter. Physically magnified ratio parameter prop up the free stream velocity which assists the velocity up

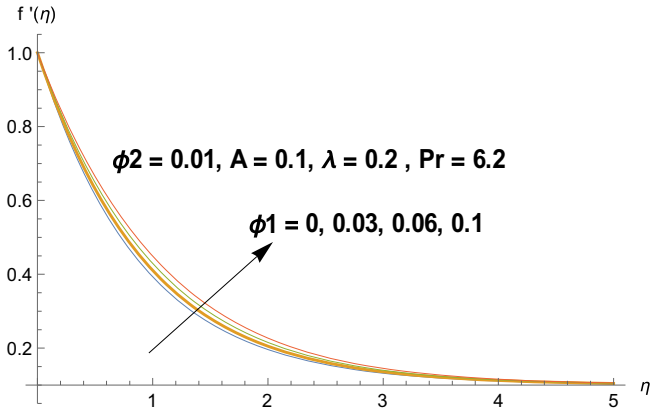


**Figure 3.** Illustration of $\Phi_1$ on $f'(\eta)$.

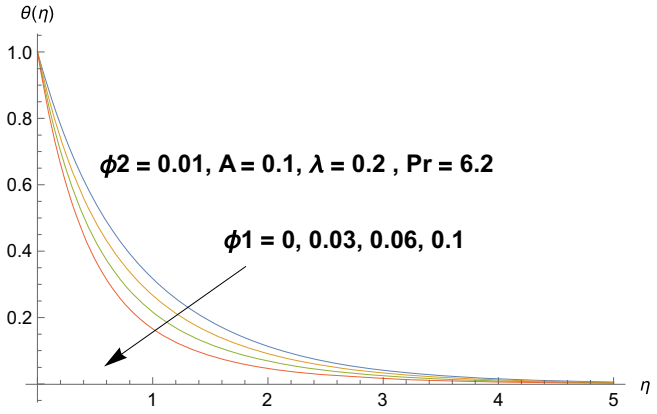


**Figure 4.** Illustration of $\Phi_1$ on $\theta(\eta)$.

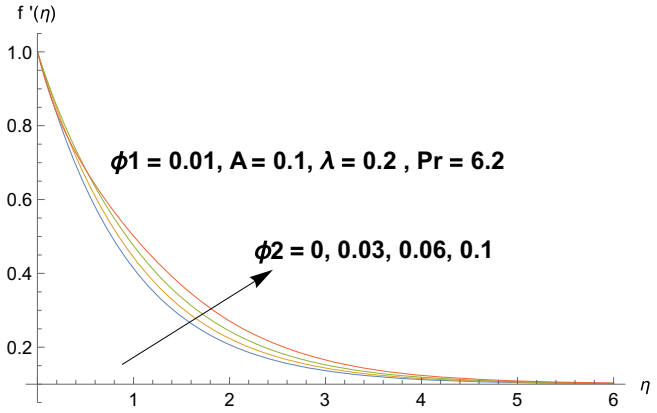


**Figure 5.** Illustration of $\Phi_2$ on $f'(\eta)$.

gradation. Figure 3 is plotted for polystyrene particles volume fraction $\Phi_1$ versus velocity profile. It is observed that velocity profile grows for enhanced polystyrene particles volume fraction. This is because nano particle concentration enhances near the plate which inturns intensifies the velocity field. Influence of polystyrene particles volume fraction on temperature profile is observed in Fig. 4. Opposite behavior is detected for velocity and temperature distributions. Both temperature profile and thermal boundary layer thickness gets steeper. Actually nanoparticles disperse in the fluid and reduces the temperature. Figure 5 depicts the behavior of titanium oxide $(TiO_2)$ particles volume fraction $\Phi_2$ on velocity field. Titanium oxide nanoparticles strengthens the velocity field. Higher concentration of titanium oxide $(TiO_2)$ particles provides significant amount of particles near the plate

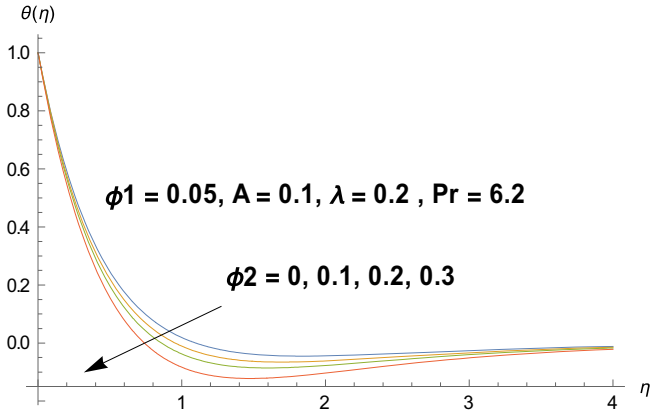


**Figure 6.** Illustration of $\Phi_2$ on $\theta(\eta)$.

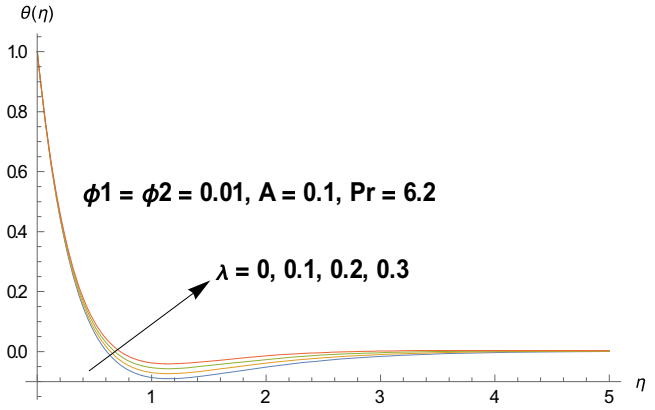


**Figure 7.** Illustration of $\lambda$ on $\theta(\eta)$.

consequently velocity increases. Figure 6 indicates the impact of titanium oxide $(TiO_2)$ particles volume fraction $\Phi_2$ on temperature distribution. Same trend is obtained as for velocity field. Nano particles volume fraction enhances the thermal conductivity of a base fluid. Therefore temperature distribution increases. Figure 7 indicates the influence of heat generation/absorption parameter $\lambda$ on temperature profile. Heat generation/absorption parameter $\lambda$ strengthens the thermal boundary layer and temperature profile. In the course of heat generation activity extra heat will be generated and eventually temperature distribution boost.

**Entropy production.** Figures 8, 9, 10, and 11 reflects the influences of various parameters on entropy generation. Figures 8 and 9 represents the effect of polystyrene particles volume fraction $\Phi_1$ and titanium oxide particles volume fraction $\Phi_2$ on entropy generation. Results shows that both polystyrene particles volume fraction and titanium oxide particles volume fraction enhances the entropy generation rate. To determine the impact of Eckert number $Ec$ on entropy generation, Fig. 10 is sketched. It is noticed that entropy generation rate is increasing function of Eckert number. Actually due to enlarged Eckert number $Ec$ supplementary heat will be induced and therefore entropy generation dominates. Figure 11 portrayed the footprints of temperature difference parameter $\Omega$ on entropy production rate. Opposite behavior has been perceived as compared to Eckert number. Entropy generation rate diminishes when temperature difference parameter grows. Figure 12 reflects the influence of velocity ratio parameter $A$ and heat generation/absorption parameter $\lambda$ on heat transfer rate. It is noticed that heat transfer rate decays for increasing velocity ratio parameter $A$ and heat generation/absorption parameter $\lambda$. Actually heat generation/absorption parameter strengthens the temperature profile. Therefore, less heat will be transferred and heat transfer rate diminishes. Figure 13 demonstrates the streamlines behavior of flow.

Nomenclature for physical parameters and symbols are given in Table 1. Table 2 represents numerical values of thermophysical properties of Polystyrene and Titanium Oxide particles (nano particles) and Table 3 express the mathematical formulation of hybrid nanofluid and base fluid. Thermal conductivity of nanofluids was proposed by Hamilton and Crosser[57]. Here n is the empirical shape factor in order to account the effect of particles shape and can be varied from 0.5 to 6.0. The shape factor n is given by $\frac{3}{\psi}$, where $\psi$ is the particles sphericity, defined as surface area of a sphere to the surface area of the particle. Therefore for spherical nanoparticles n = 3. This case of Hamilton and Crossere model (n = 3) is the same as Maxwell model[58]. Similarly density,specific heat

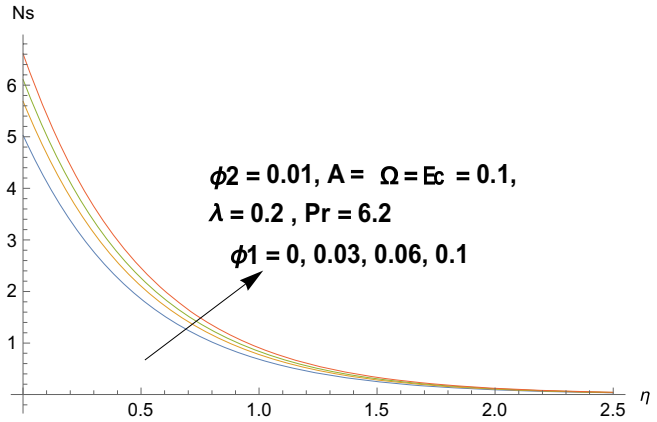


**Figure 8.** Illustration of $\Phi_1$ on $N_s$.

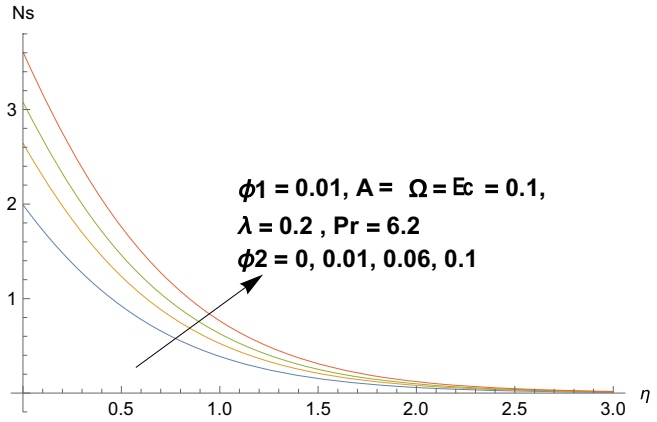


**Figure 9.** Illustration of $\Phi_2$ on $N_s$.

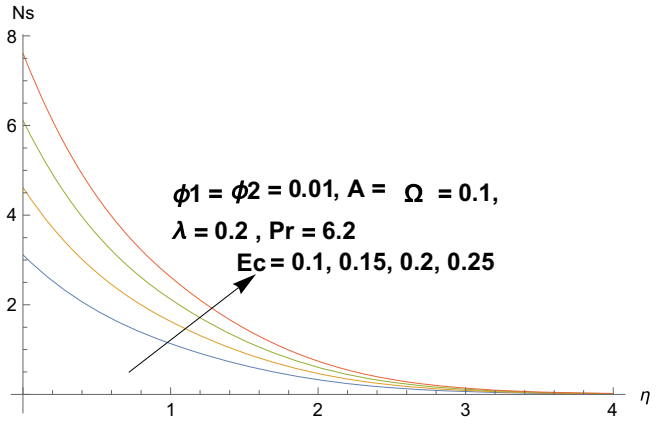


**Figure 10.** Illustration of *Ec* on $N_s$.

and dynamic viscosity of hybrid nanoparticles were used in literature[59–61]. Table 4 expresses the numerical values of skin friction coefficient for different physical parameters. It is observed that drag force decreases for both $\Phi_1$ (nano particle volume fraction of polystyrene) and $\Phi_2$ (nano particle volume fraction of titanium Oxide). Physically, increase in velocity profile educes the drag force for $\Phi_1$ and $\Phi_2$. Whereas opposite behavior is noticed for $A$ (velocity ratio parameter). Table 5 shows the numerical values of heat transfer rate for unlike physical

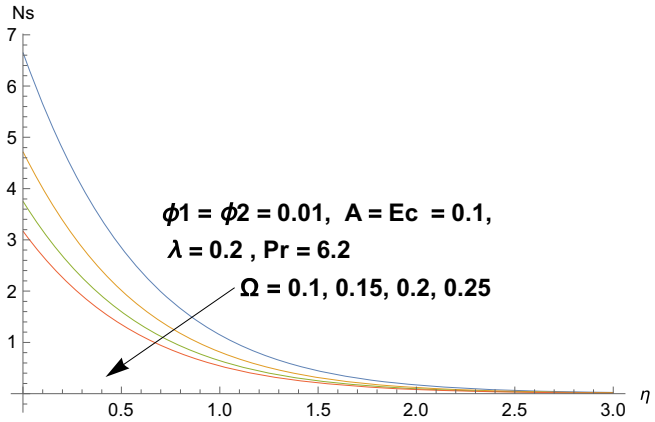


**Figure 11.** Illustration of Ω on $N_s$.

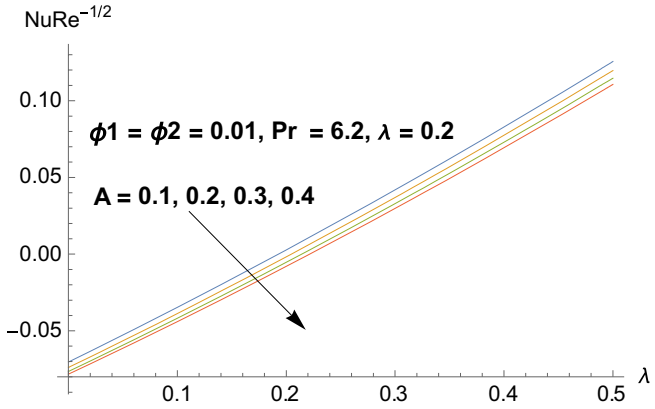


**Figure 12.** Illustration of A and $\lambda$ on $_{Nu}\mathrm{Re}^{-1}/_{2}$.

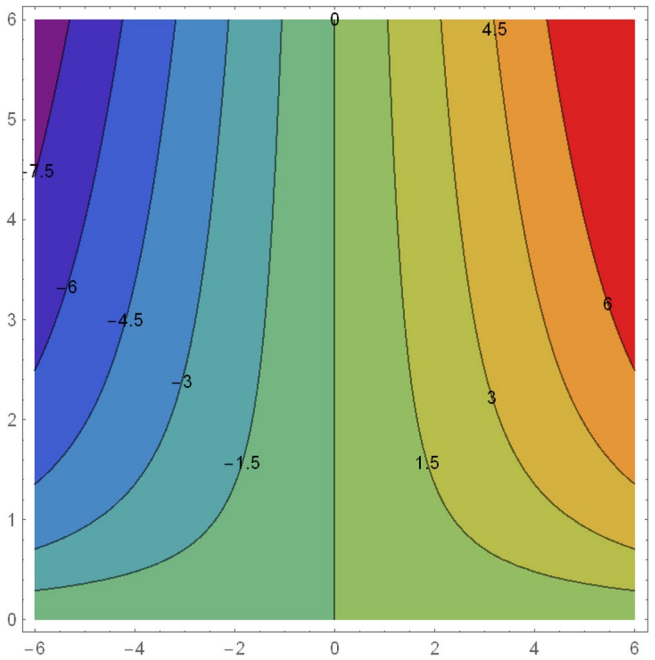


**Figure 13.** Flow pattern for streamlines.

| Nomenclature | |
|---|---|
| $k_f$ | Thermal conductivity of water ($Wm^{-1}\ K^{-1}$) |
| $k_{nf}$ | Thermal conductivity of nanofluid ($Wm^{-1}\ K^{-1}$) |
| $k_{hnf}$ | Thermal conductivity of hybrid nanofluid ($Wm^{-1}\ K^{-1}$) |
| $k_{s1}$ | Thermal conductivity of polystyrene ($Wm^{-1}\ K^{-1}$) |
| $k_{s2}$ | Thermal conductivity of Titanium Oxide ($Wm^{-1}\ K^{-1}$) |
| $a, b$ | Dimensionless constants |
| $f'$ | Dimensionless velocity |
| $T$ | Fluid temperature (K) |
| $T_0$ | Reference temperature (K) |
| $T_\infty$ | Ambient temperature (K) |
| $T_w$ | Surface temperature (K) |
| $U_w(x)$ | Stretching velocity ($m\ s^{-1}$) |
| $U_e(x)$ | Free stream velocity ($m\ s^{-1}$) |
| Pr | Prandtl number |
| $A$ | Velocity ratio parameter |
| $\lambda$ | Heat generation/absorption parameter |
| $Q$ | Heat generation/absorption coefficient |
| $C_f$ | Local skin friction coefficient |
| $Re_x$ | Local Reynold number |
| $Nu$ | Nusselt number |
| $q_w$ | Heat flux |
| **Greek symbols** | |
| $\rho_f$ | Density of water ($kg\ m^{-3}$) |
| $\rho_{nf}$ | Density of nanofluid ($kg\ m^{-3}$) |
| $\rho_{hnf}$ | Density of hybrid nanofluid ($kg\ m^{-3}$) |
| $\rho_{s1}$ | Density of polystyrene ($kg\ m^{-3}$) |
| $\rho_{s2}$ | Density of titanium oxide ($kg\ m^{-3}$) |
| $\mu_f$ | Dynamic viscosity of water ($kg\ m^{-1}\ s^{-1}$) |
| $\mu_{hnf}$ | Dynamic viscosity of hybrid nanofluid ($kg\ m^{-1}\ s^{-1}$) |
| $\alpha_{hnf}$ | Thermal diffusivity of hybrid nanofluid ($m^2 s^{-1}$) |
| $\upsilon_{hnf}$ | Kinematic viscosity of hybrid nanofluid ($m^2 s^{-1}$) |
| $\eta$ | Similarity variable |
| $\Phi_1$ | Nano particle volume concentration of polystyrene |
| $\Phi_2$ | Nano particle volume concentration of $TiO_2$ |
| $(\rho C)_f$ | Specific heat of water ($J\ K^{-1}\ m^{-3}$) |
| $(\rho C)_{hnf}$ | Specific heat of hybrid nanofluid ($J\ K^{-1}\ m^{-3}$) |
| $(\rho C)_{s1}$ | Specific heat of polystyrene ($J\ K^{-1}\ m^{-3}$) |
| $(\rho C)_{s2}$ | Specific heat of $TiO_2$ ($J\ K^{-1}\ m^{-3}$) |
| $\theta$ | Dimensionless temperature |
| $\tau_w$ | Wall shear stress ($kg\ 3^{-1}\ s^{-2}$) |

**Table 1.** Nomenclature table for physical parameters and symbols[54].

| Base fluid/nano particles | $\rho$ ($kg\ m^{-3}$) | $C_p$ ($J\ K^{-1}$) | $k$ ($W\ K^{-1}\ m^{-1}$) |
|---|---|---|---|
| Water ($H_2O$) | 997.1 | 4179 | 0.613 |
| Polystyrene | 1053 | 1210 | 0.16 |
| Titanium Oxide ($TiO_2$) | 4250 | 686.2 | 8.9538 |

**Table 2.** Thermo physical properties of base fluid and nano particles[65,66].

parameters. Decay in rate of heat transfer is noticed for enlarged $\Phi_1$ (nano particle volume fraction of polystyrene) whereas increasing trend is observed for $\Phi_2$ (nano particle volume fraction of titanium Oxide) and $\lambda$ (heat generation/absorption parameter). Table 6 is prepared for the analysis of surface drag coefficient ($f''(0)$) with published works of Mahapatra and Gupta[62], Pop et al.[63], Sharma and Singh[64] and Masood et al.[55] in limiting case. Both results are in good manner.

| Properties | Hybrid nanofluid |
|---|---|
| Dynamic viscocity (N s $m^{-2}$) | $\mu_{hnf} = \frac{\mu_f}{(1-\Phi_1)^{2.5}(1-\Phi_2)^{2.5}}$ |
| Density (kg $m^{-3}$) | $\rho_{hnf} = [(1-\Phi_2)\{(1-\Phi_1)\rho_f + \Phi_1\rho_{s1}\} + \Phi_2\rho_{s2}]$ |
| Thermal conductivity (W $K^{-1}$ $m^{-1}$) | $\frac{k_{hnf}}{k_{nf}} = \frac{k_{s2}+(n-1)k_{nf}-(n-1)\Phi_2(k_{nf}-k_{s2})}{k_{s2}+(n-1)k_{nf}+\Phi_2(k_{nf}-k_{s2})}$ where $\frac{k_{nf}}{k_f} = \frac{k_{s1}+(n-1)k_f-(n-1)\Phi_1(k_f-k_{s1})}{k_{s1}+(n-1)k_f+\Phi_1(k_f-k_{s1})}$ |
| Heat capacity (J $K^{-1}$) | $[(1-\Phi_2)\{(1-\Phi_1)(\rho C_p)_f + \Phi_1(\rho C_p)_{s1}\} + \Phi_2(\rho C_p)_{s2}]$ |

**Table 3.** Mathematical formulation of thermo physical properties of hybrid nanofluid[67–70].

| $\Phi_1$ | $\Phi_2$ | $A$ | $f''(0)$ |
|---|---|---|---|
| 0.01 | 0.01 | 0.1 | 0.0042989 |
| 0.02 | | | 0.0037307 |
| 0.03 | | | 0.0031260 |
| 0.01 | | | 0.0042989 |
| | 0.02 | | 0.0040934 |
| | 0.03 | | 0.003915 |
| | 0.01 | | 0.0042989 |
| | | 0.2 | 0.0073951 |
| | | 0.3 | 0.013953 |

**Table 4.** Skin friction coefficient for different parameters when $\lambda = 0.1, Pr = 6.2$.

| $\Phi_1$ | $\Phi_2$ | $\lambda$ | $-\theta'(0)$ |
|---|---|---|---|
| 0.01 | 0.01 | 0.1 | 0.015735 |
| 0.02 | | | 0.015511 |
| 0.03 | | | 0.015359 |
| 0.01 | | | 0.015735 |
| | 0.02 | | 0.016164 |
| | 0.03 | | 0.016529 |
| | 0.01 | | 0.015735 |
| | | 0.2 | 0.015838 |
| | | 0.3 | 0.016084 |

**Table 5.** Nusselt number for different parameters when $A = 0.1, \mathrm{Pr} = 6.2$.

| A | Mahapatra and Gupta[62] | Pop et al.[63] | Sharma and Singh[64] | Masood et al.[55] | Present results |
|---|---|---|---|---|---|
| 0.1 | −0.9694 | −0.9694 | −0.969483 | −0.96939 | −0.96939 |
| 0.2 | −0.9181 | −0.9181 | −0.9181069 | −0.91811 | −0.91811 |
| 0.5 | −0.6673 | −0.6673 | −0.667263 | −0.66726 | −0.66726 |

**Table 6.** Review of skin friction coefficient ($f''(0)$) with previous published work of Mahapatra and Gupta[62], Pop et al.[63], Sharma and Singh[64] and Masood et al.[55] for different values of $A$ when $\Phi_1 = \Phi_2 = 0$.

## Conclusions

Influence of heat generation/absorption and stagnation point on hybrid nanofluid are taken into account. Hybrid nanofluid contains Polystyrene and $TiO_2$ nanoparticles with water as a transiet fluid. The disruptive results for the sophisticated parameters are displayed graphically. The majour outcomes are as persued.

- Volume fraction of polystyrene particles $\Phi_1$ enlarged the velocity profile and degrade the temperature profile.
- Volume fraction of titanium oxide $\Phi_2$ particles magnifies the velocity field.

- Velocity ratio parameter enhanced the velocity field.
- Heat generation/absosption parameter emlarged the temperature profile.
- Entropy generation intensifies for both polystyrene and titanium oxide parcticles.
- Eckert number *Ec* also amplifies the entropy generation strength.
- Temperature difference parameter decays the entropy generation.

The preference is that the contemporaneous analysis will be extremely beneficial for modeling better flow obstacles specifically in biomedical industry, for cancer treatment, aerodynamic industry, power generation, nuclear reactors and solar thermal absorbers.

Received: 23 February 2021; Accepted: 26 October 2021
Published online: 17 November 2021

## References

1. Choi, S.U.S. Enhancing thermal conductivity of fluids with nanoparticles. in *The Proceedings of the ASME International Mechanical Engineering Congress and Exposition*, Vol. 66, 99–105 (San Francisco, 1995)
2. Waini, I., Ishak, A. & Pop, I. Transpiration effects on hybrid nanofluid flow and heat transfer over a stretching/shrinking sheet with uniform shear flow. *Alex. Eng. J.* **59**, 91–99 (2020).
3. Tassaddiq, A. *et al.* Heat and mass transfer together with hybrid nanofluid flow over a rotating disk. *AIP. Adv.* https://doi.org/10.1063/5.0010181 (2020).
4. TayebI, T., Öztop, H. F. & Chamkha, A. J. Natural convection and entropy production in hybrid nanofluid filled-annular elliptical cavity with internal heat generation or absorption. *Therm. Sci. Eng. Prog.* https://doi.org/10.1016/j.tsep.2020.100605 (2020).
5. Zahid, U. M., Akbar, Y. & Abbasi, F. M. Entropy generation analysis for peristaltically driven flow of hybrid nanofluid. *Chin. J. Phy.* **67**, 330–348 (2020).
6. Yusuf, T. A., Mabood, F., Khan, W. A. & Gbadeyan, J. A. Irreversibility analysis of Cu-TiO2-H2O hybrid-nanofluid impinging on a 3-D stretching sheet in a porous medium with nonlinear radiation: Darcy–Forchhiemer's model. *Alex. Eng. J.* **59**, 5247–5261 (2020).
7. Wanatasanapan, V. V., Abdullah, M. Z. & Gunnasegaran, P. Effect of $TiO_2$–$Al_2O_3$ nanoparticle mixing ratio on the thermal conductivity, rheological properties, and dynamic viscosity of water-based hybrid nanofluid. *J. Mater. Res. Technol.* **9**, 13781–13792 (2020).
8. Said, Z. *et al.* Heat transfer, entropy generation, economic and environmental analyses of linear Fresnel reflector using novel rGO-$Co_3O_4$ hybrid nanofluids. *Renew. Energy.* https://doi.org/10.1016/j.renene.2020.11.054 (2020).
9. Abbas, N. *et al.* Models base study of inclined MHD of hybrid nanofluid flow over nonlinear stretching cylinder. *Chin. J. Phys.* https://doi.org/10.1016/j.cjph.2020.11.019 (2020).
10. Arani, A. A. A. & Aberoumand, H. Stagnation-point flow of Ag–CuO/water hybrid nanofluids over a permeable stretching/shrinking sheet with temporal stability analysis. *Powder. Technol.* https://doi.org/10.1016/j.powtec.2020.11.043 (2020).
11. Li, X., Indumathi, N., Wang, H. & Luo, B. The thermophysical properties and enhanced heat transfer performance of SiC-MWCNTs hybrid nanofluids for car radiator system. *Colloids. Surf A. Physicochem. Eng. Asp.* https://doi.org/10.1016/j.colsurfa.2020.125968 (2020).
12. Waini, I., Ishak, I. & Pop, I. Squeezed hybrid nanofluid flow over a permeable sensor surface. *Mathematics.* **8**(6), 898. https://doi.org/10.3390/math8060898 (2020).
13. Waini, I., Ishak, I. & Pop, I. Hybrid nanofluid flow on a shrinking cylinder with prescribed surface heat flux. *Int. J. Numer. Method. H.* **31**(6), 1987–2004 (2020).
14. Zhang, J., Wang, X., Lu, L., Li, D. & Yang, X. Preparation and performance of high impact polystyrene(HIPS)/Nano-$TiO_2$ nanocomposites. *J. Appl. Polym. Sci.* **87**, 381–385 (2003).
15. Zan, L., Tian, L., Liu, Z. & Peng, Z. A new polystyrene–$TiO_2$ nanocomposite film and its photocalytic degradation. *Appl. Catal. A. Gen.* **264**, 237–242 (2004).
16. Wang, Z., Li, G., Peng, H. & Zhang, Z. Study on novel antibacterial high impact polystyrene/$TiO_2$ nanocomposites. *J. Mater. Sci.* **40**, 6433–6438 (2005).
17. Zhang, Q., Peng, H. & Zhang, Z. Antibacteria and detoxification function of polystyrene/$TiO_2$ nanocomposites. *J. Dispers. Sci. Technol.* **28**, 937–941 (2007).
18. Sang, X., Peng, W., Chen, X. & Hou, G. Effect of core-shell particles on the properties of polystyrene/$TiO_2$ nanocomposites. *Adv. Mat. Res.* **139–141**, 90–93 (2010).
19. Naganthran, K., Nazar, R. & Pop, I. Stability analysis of impinging oblique stagnation-point flow over a permeable shrinking surface in a viscoelastic fluid. *Int. J. Mech. Sci.* **131**, 663–671 (2017).
20. Khan, M. I., Hayat, T., Shah, F., Rahman, M. & Haq, F. Physical aspects of CNTs and induced magnetic flux in stagnation point flow with quartic chemical reaction. *Int. J. Heat. Mass. Transf.* **135**, 561–568 (2019).
21. Ahmed, J., Khan, M. & Ahmad, L. Stagnation point flow of Maxwell nanofluid over a permeable rotating disk with heat source/sink. *J. Mol. Liq.* **287**, 110853 (2019).
22. Moshkin, N. P., Pukhnachev, V. V. & Bozhkov, Y. D. On the unsteady, stagnation point flow of a Maxwell fluid in 2D. *Int. J. Non Linear. Mech.* **116**, 32–38 (2019).
23. Weidman, P. Hiemenz stagnation-point flow impinging on a uniformly rotating plate. *Eur. J. Mech. B Fluids.* **78**, 169–173 (2019).
24. Mahapatra, T. R. & Sidui, S. Non-axisymmetric Homann stagnation-point flow of a viscoelastic fluid towards a fixed plate. *Eur. J. Mech. B Fluids.* **79**, 38–43 (2019).
25. Azhar, E., Iqbal, Z. & Maraj, E. N. Viscous dissipation performance on stagnation point flow of Jeffrey fluid inspired by internal heat generation and chemical reaction. *Therm. Sci. Eng. Prog.* **13**, 100377 (2019).
26. Chu, Y. M. *et al.* Transportation of heat and mass transport in hydromagnetic stagnation point flow of Carreau nanomaterial: Dual simulations through Runge–Kutta Fehlberg technique. *Int. Commun. Heat. Mass Transf.* **118**, 104858 (2020).
27. Shah, F., Khan, M. I., Hayat, T., Momani, S. & Khan, M. I. Cattaneo–Christov heat flux (CC model) in mixed convective stagnation point flow towards a Riga plate. *Comput. Meth. Programs. Biomed.* https://doi.org/10.1016/j.cmpb.2020.105564 (2020).
28. Awan, A. U., Abid, S., Ullah, N. & Nadeem, S. Magnetohydrodynamic oblique stagnation point flow of second grade fluid over an oscillatory stretching surface. *Results. Phys.* **18**, 103233 (2020).
29. Waini, I., Ishak, I. & Pop, I. Hybrid nanofluid flow towards a stagnation point on a stretching/shrinking cylinder. *Sci. Rep.* **10**, 9296. https://doi.org/10.1038/s41598-020-66126-2 (2020).
30. Zainal, N. A., Nazar, I., Naganthran, K. & Pop, I. Unsteady MHD mixed convection flow in hybrid nanofluid at three dimensional stagnation point. *Mathematics.* https://doi.org/10.3390/math9050549 (2020).
31. Waini, I., Ishak, I. & Pop, I. Hybrid nanofluid flow towards a stagnation point on an exponentially stretching/shrinking vertical sheet with buoyancy effects. *Int. J. Numer. Method. H.* https://doi.org/10.1108/HFF-02-2020-0086 (2020).

32. Khashi'ie, N. S., Waini, I., Zainal, N. A., Hamzah, K. & Kasim, A. R. M. Hybrid nanofluid flow past a stretching cylinder with prescribed surface heat flux. *Symmetry.* **12**, 1493. https://doi.org/10.3390/sym12091493 (2020).
33. Zainal, N. A., Nazar, I., Naganthran, K. & Pop, I. Unsteady stagnation point flow of hybrid nanofluid past a convectively heated stretching/shrinking sheet with slip velocity. *Mathematics.* **8**, 1649. https://doi.org/10.3390/math8101649 (2020).
34. Zainal, N. A., Nazar, I., Naganthran, K. & Pop, I. Viscous dissipation and Mhd hybrid nanofluid flow towards an exponentially stretching/shrinking surface. *Neural. Comput. Appl.* https://doi.org/10.1007/s00521-020-05645 (2020).
35. Zainal, N. A., Nazar, I., Naganthran, K. & Pop, I. Stability analysis of Mhd hybrid nanofluid flow over a stretching/shrinking sheetwith quadratic velocity. *Alex. Eng. J.* **60**, 915–926 (2021).
36. Ibrahim, W. & Gadisa, G. Finite element solution of nonlinear convective flow of Oldroyd-B fluid with cattaneo-christov heat flux model over nonlinear stretching sheet with heat generation or absorption. *Propuls. Power. Res.* **9**(3), 304–315 (2020).
37. Zainal, N. A., Nazar, R., Naganthran, K. & Pop, I. Heat generation/absorption effect on MHD flow of hybrid nanofluid over bidirectional exponential stretching/shrinking sheet. *Chin. J. Phys.* https://doi.org/10.1016/j.cjph.2020.12.002 (2020).
38. Hafeez, A. & Khan, M. Flow of Oldroyd-B fluid caused by a rotating disk featuring the cattaneo-christov theory with heat generation/absorption. *Int. Commun. Heat. Mass.* **123**, 105179 (2021).
39. Tayabi, T., Chamkha, A. J., Melaibari, A. A. & Raouache, E. Effect of internal heat generation or absorption on conjugate thermal free convection of a suspension of hybrid nanofl;uid in a portioned circular annulus. *Int. Commun. Heat. Mass.* **126**, 105397 (2021).
40. Bejan, A. A study of entropy generation in fundamental convective heat transfer. *J. Heat. Trans.* **101**, 718–725 (1979).
41. Gholamalipour, P., Siavashi, M. & Doranehgard, M. H. Eccentricity effects of heat source inside a porous annulus on the natural convection heat transfer and entropy generation of Cu–water nanofluid. *Int. Commun. Heat. Mass. Transfer.* **109**, 104367 (2019).
42. Dutta, S., Goswami, N., Biswas, A. K. & Pati, S. Numerical investigation of magnetohydrodynamic natural convection heat transfer and entropy generation in a rhombic enclosure filled with Cu–water nanofluid. *Int. J. Heat. Mass. Transf.* **136**, 777–798 (2019).
43. Khan, A., Shah, Z., Alzahrani, E. & Islam, S. Entropy generation and thermal analysis for rotary motion of hydromagnetic Casson nanofluid past a rotating cylinder with Joule heating effect. *Int. Commun. Heat. Mass Transf.* **119**, 104979 (2020).
44. Ambreen, A., Saleem, A. & Park, C. W. Analysis of hydro-thermal and entropy generation characteristics of nanofluid in an aluminium foam heat sink by employing Darcy–Forchheimer–Brinkman model coupled with multiphase Eulerian model. *Appl. Therm. Eng.* **173**, 115231 (2020).
45. Cho. C. C. Effects of porous medium and wavy surface on heat transfer and entropy generation of Cu-water nanofluid natural convection in square cavity containing partially-heated surface. Int. Commun. Heat. Mass. Transf. 119, 104925. (2020).
46. Li, Z., Hussein, A. K., Younis, O., Afrand, M. & Feng, S. Natural convection and entropy generation of a nanofluid around a circular baffle inside an inclined square cavity under thermal radiation and magnetic field effects. *Int. Commun. Heat. Mass Transf.* **116**, 104650 (2020).
47. Sáchica, D., Treviño, C. & Suástegui, L. M. Numerical study of magnetohydrodynamic mixed convection and entropy generation of $Al_2O_3$–water nanofluid in a channel with two facing cavities with discrete heating. *Int. J. Heat. Fluid. Flow.* **86**, 108713 (2020).
48. Liao, S. J. Notes on the Homotopy Analysis Method: Some definitions and theorem. *Commun. Nonlinear. Sci.* **14**, 983–997 (2009).
49. Hayat, T., Qayyum, S., Imtiaz, M. & Alsaedi, A. Flow between two stretchable rotating disks with Cattaneo–Christov heat flux model. *Result. Phys* **7**, 126–133 (2017).
50. Shirkhani, M. R., Hoshyara, H. A., Rahimipetroudi, I., Akhavan, H. & Ganji, D. D. Unsteady time-dependent incompressible Newtonian fluid flow between two parallel plates by homotopy analysis method (HAM), homotopy perturbation method (HPM) and collocation method (CM). *Propuls. Power. Res.* **7**, 247–256 (2018).
51. Jafarimoghaddam, A. On the Homotopy Analysis Method (HAM) and Homotopy Perturbation Method (HPM) for a nonlinearly stretching sheet flow of Eyring-Powell fluids. *Eng. Sci. Technol. Int. J.* **22**, 439–451 (2018).
52. Masood, S., Farooq, M. & Ahmad, S. Description of viscous dissipation in magnetohydrodynamic flow of nanofluid flow: Applications of biomedical treatment. *Adv. Mech. Eng.* **12**, 1–13 (2020).
53. Ahmad, S., Farooq, M., Rizwan, M., Ahmad, B. & Rehman, S. Melting phenomenon in a squeezed rheology of reactive rate type fluid. *Front. Phys.* https://doi.org/10.3389/fphy.2020.00108 (2020).
54. Masood, S. & Farooq, M. Influence of thermal stratification and thermal radiation on graphene oxide-Ag/$H_2O$ hybrid nanofluid. *J. Therm. Anal. Calorim.* **143**, 1361–1370 (2021).
55. Masood, S., Farooq, M., Ahmad, S., Anjum, A. & Mir, N. A. Investigation of viscous dissipation in the nanofluid flow with a Forchheimer porous medium: Modern transportation of heat and mass. *Eur. Phys. J. Plus.* **134**, 178 (2019).
56. Shafique, Z., Mustafa, M. & Mushtaq, A. Boundary layer flow of Maxwell fluid in rotating frame with binary chemical reaction and activation energy. *Result. Phys.* **6**, 627–633 (2016).
57. Hamilton, R. L. & Crosser, O. K. Thermal conductivity of heterogeneous two component systems. *Ind. Eng. Chem.* **1**(3), 187–191 (1962).
58. Maxwell, J. C. *A Treastise on Electricity and Magnetism* (OUP, 1881).
59. Ben-Mansour, R. & Habib, M. A. Use of nanofluids for improved natural coolinf of discretely heated cavities. *Adv. Mech. Eng.* **2013**, 383267 (2013).
60. Rostamani, M., Hosseinizadeh, S. F., Gorji, M. & Khodadadi, J. M. Numerical study of turbulent forced convection flow of nanofluids in a long horizontal duct considering variable properties. *Int. Commun. Heat Mass Transf.* **37**(10), 1426–1431 (2010).
61. Bianco, V., Manca, O. & Nardini, S. Numerical investigation on nanofluids turbulent convection heat transfer inside a circular tube. *Int. Therm. Sci.* **50**(3), 341–349 (2011).
62. Mahapatra, T. R. & Gupta, A. Heat transfer in stagnation point flow towards a stretching sheet. *Heat. Mass. Transf.* **38**, 517–521 (2002).
63. Pop, S., Grosan, T. & Pop, I. Radiation effects on the flow near the stagnation point of a stretching sheet. *Tech. Mech.* **25**, 100–106 (2004).
64. Sharma, P. & Singh, G. Effects of variable thermal conductivity and heat source/sink on MHD flow near a stagnation point on a linearly stretching sheet. *J. Appl. Fluid Mech.* **2**, 13–21 (2009).
65. Sheikholeslami, M., Hatami, M. & Ganji, D. D. Nanofluid flow and heat transfer in a rotating system in the presence of a magnetic field. *J. Mol. Liq.* **190**, 112–120 (2014).
66. Khan, M. I., Hafeez, M. U., Hayat, T., Khan, M. I. & Alsaedi, A. Magneto rotating flow of hybrid nanofluid with entropy generation. *Comput. Biool. Med.* **183**, 105093 (2020).
67. Sarkar, J., Ghosh, P. & Adil, A. A review on hybrid nanofluids: Recent research, development and applications. *Renew. Sust. Energ. Rev.* **43**, 164–177 (2015).
68. Sundar, L. S., Sharma, K. V., Singh, M. K. & Sousa, A. C. M. Hybrid nanofluids preparation, thermal properties, heat transfer and friction factor—A review. *Renew. Sust. Energy. Rev.* **68**, 185–198 (2017).
69. Sidik, N. A. C., Jamil, M. M., Japar, W. M. A. A. & Adamu, I. M. A review on preparation methods, stability and applications of hybrid nanofluids. *Renew. Sust. Energ. Rev.* **80**, 1112–1122 (2017).
70. Afrand, M., Najafabadi, K. N. & Akbari, M. Effects of temperature and solid volume fraction on viscosity of $SiO_2$-MWCNTs/SAE 40 hybrid nanofluid as a coolant and lubricant in heat engines. *Appl. Therm. Eng.* **102**, 45–54 (2016).

## Author contributions

S.M. and M.F. wrote the main manuscript text and S.M. prepared figures and tables. Both authors revised the manuscript. A.A. helped for preparing revised manuscript.

## Competing interests

The authors declare no competing interests.

## Additional information

**Correspondence** and requests for materials should be addressed to S.M.

**Reprints and permissions information** is available at www.nature.com/reprints.

**Publisher's note** Springer Nature remains neutral with regard to jurisdictional claims in published maps and institutional affiliations.